ERCNN-DRM: an efficient regularized convolutional neural network with a dimensionality reduction module for the classification of brain tumour in magnetic resonance images

Selvin Prem Kumar S, Agees Kumar C & Jemila Rose R

Published online: 08 Aug 2022.

Submit your article to this journal ⬀

Article views: 323

View related articles ⬀

View Crossmark data ⬀

Taylor & Francis
Taylor & Francis Group

REGULAR PAPER

🔓 OPEN ACCESS   ⟳ Check for updates

ERCNN-DRM: an efficient regularized convolutional neural network with a dimensionality reduction module for the classification of brain tumour in magnetic resonance images

Selvin Prem Kumar S[a], Agees Kumar C[b] and Jemila Rose R[c]

[a]Department of Computer Science and Engineering, CSI Institute of Technology, Thovalai, Tamil Nadu, India; [b]Department of EEE, Arunachala College of Engineering for Women, Nagercoil, Tamil Nadu, India; [c]Department of CSE, St. Xavier's Catholic College of Engineering, Nagercoil, Tamil Nadu, India

ABSTRACT

Brain tumour is a severe disease that may lead to death if unrecognized and untreated. Brain tumor identification and segmentation is a complex and task in medical image processing. For radiologists, diagnosing and classifying tumor from various images is a challenging process. When the data size is large, deep learning methods outperform conventional learning algorithms. Convolutional Neural Networks are found to be one of the popular deep learning architectures. We propose a deep network with an Efficient Regularized CNN with Dimensionality Reduction Module (ERCNN-DRM), which works with less training data and produces more precise classification with minimal processing time and regularisation. The images are pre-processed, segmented and then the dimension reduced features are extracted using the proposed algorithms and then the proposed regularized classification takes place. The experiment is conducted on TCIA dataset which contains a total of 696 MRI, 224 of which are benign and 472 of which are malignant. The proposed scheme produces accuracy rate of 96.7% and reduces the complexity by working on dimensional reduced data. Performance measures such as accuracy, recall, precision, F-measures are analysed and the system is found to be significant than other state-of-the art.

1. Introduction

The brain tumour is an irregular development of brain tissue that may cause life loss in humans if left undetected. It should be diagnosed and properly treated at an early stage [1]. Till the signs have been noticed, tit can grow very large. Usually, MRI (Magnetic Resonance Images) and CT (Computer Tomography) images are preferred by radiologists to diagnose brain tumours [2]. The tumour may increase the brain pressure, force the brain against the skull, invading and destroying healthy brain tissue and nerves. The type of symptom detected is determined by the location of the brain tumour. This is because the same functions are regulated by various parts of the brain. Tumour types vary from person to person. They can be developed in a variety of ways, mature from several cell types and receive many treatments. Tumours may be benign and malign. The malign tumours are more dangerous than benign ones, and may grow fast and spread to other areas of the brain and spine [3]. Diagnosing the brain tumour and its type is a complicated and long process. The diagnosis of brain tumours can be aided by image processing techniques. Tumour treatment can be done with surgery,

chemotherapy, or radiation, only after the diagnosis. Hence, diagnosis is an important phase.

MRI is used to identify tumours, because it is a better imaging technique, and also offers knowledge about soft tissue organization in humans. It is used to analyze the human body organization. Furthermore, MRI is more important and useful in medical imaging, because it provides different changes, within the various soft tissues [4]. It plays a vital role in advanced scientific studies of the human brain. MRI may reveal important details about the structure of soft tissues. It also contributes greatly to the precision of identification and the advancement of brain pathology. The amount of data required for manual interpretation is excessively large, necessitating the use of computerized image analysis [5].

The captured images are processed using software-oriented algorithms, to distinguish the suspicious area of the tumour, from the safe area in the image. The obtained features of an MRI image are the most important component because it represents an image in its compact format. More feature extraction methods are also used, allowing classifiers to categorize the tumour

---

CONTACT Selvin Prem Kumar S ✉ selvinresearch@gmail.com 🌐 Department of ECE, CSI Institute of Technology, Thovalai, Kanyakumari, Tamil Nadu, India

as benign or malign [6]. Compared to CT scan and X-ray, MRI provides more flexibility. The benefit of MRI is that it does not require radiation, which is harmful to the human body [7]. Computer Aided Diagnosis (CAD) [8–10] can be used for automatic detection. Many researchers have recently presented various techniques for detecting and segmenting the tumour area in MRI [11].

The treatment is assisted by the specific segmentation method, which helps in assessing the tumour's location to scale. Hence image segmentation is a crucial process. Manual segmentation is a challenging and time-consuming task. Therefore, some trained algorithms used to segment the targeted area have been proposed in Ref. [12]. Various researchers have studied many segmentation techniques and classifiers [13–18]. Mishra et al. [19] described the Discrete Wavelet Transform (DWT), GLCM (Gray-Level Co-Occurrence Matrix), and Gabor wavelet for brain tumour segmentation and categorization. In the pre-processing portion, the Ostu thresholding is carried out initially. The tumour portions are detected using K-means clustering. Similarly, the GLCM, DWT, and Gabor wavelet were used to perform various functions. Shen et al. [20] have proposed Conditional Random Fields and Concurrent FCNs to perform the tumour segmentation. This article explains MRI brain tumour segmentation, which included pre-processing, segmentation, and post-processing. The Median filter, Gaussian filter, and Gabor filter were chosen for pre-processing phase, but they resulted in blurred borders and edges and consumed a long time.

Machine Learning (ML) is the study of algorithms and mathematical models used to carry out a task, without the use of explicit instructions, but relying on patterns, and it is used in the medical field as a part of AI. It is of two types: supervised and unsupervised [21]. Deep Learning (DL) is a subset of machine learning that is focused on learning hierarchical feature learning and learning data representations. For feature extraction, DL algorithms employ a system of multiple layers of nonlinear processing identities. Each sequential layer's output forms the next layer's input. As we move further into the network, this aids in data abstraction [22,23]. Among deep learning methods, CNN is a better method. Razak et al. [24] proposed two-path-way group of conventional networks, showing 80% sensitivity. The ability of CNNs to learn complex feature representations by themselves, using their convolutional layers is a key reason for their success. Cui et al. [25] and Alhichri et al. [26] have proposed a multi-scale deep neural network, implemented with a SqueezeNet CNN that performs similarly to AlexNet CNN, which shows 93.46% of accuracy. In 2018, Chelghoum et al. [27] proposed nine-deep CNN architectures for feature extraction: AlexNet, GoogleNet, VGG16, VGG19, Residual Networks, Residual Networks and Inception-v2, and

Squeeze and Excitation Network, showing an accuracy of 90%. In 2019, Sunanda Das et al. [28] proposed a CNN architecture with an accuracy rate of 94.39% to detect glioma brain tumours and classify them into three types. Sriramakrishnan et al. [29] have used multi-sequence MRI datasets, accessible from BraTS, and the article establishes a rapid and automated method for brain tumour detection and segmentation. The proposed method is divided into three phases: identification of tumorous slices, tumour extraction, and tumour substructure segmentation. The MRI slices are categorized using feature blocks and an SVM classifier. The Fuzzy C Means algorithm is used to separate tumour area, and the tumour substructures are segmented using a probabilistic local ternary patterns (PLTP) technique. Al-Tamimi et al. [30] have developed a threshold-based approach for brain tumour detection, based on measures such as mean, energy, and entropy. The existing work has the benefit that CNN-based algorithms can learn complex feature representations by themselves utilizing their convolutional layers. The following are some of the drawbacks of present brain tumour classification methods. Given the medical importance of the classification problem, the performance of state-of-the-art algorithms [25,27] is insufficient. Before classification, earlier approaches depended on manually drawn tumour sections. They were unable to be fully mechanized as a result of this. Existing automatic algorithms based on CNN and its derivatives have not been able to significantly increase performance.

Problem statement:

In brain tumour diagnosis, segmentation of tumour and classifying them into benign or malign is important. Previous systems need great improvement to increase tumour detection precision, applicability, and automation and they require work on large training data, thus making the system complex. Some computerized classification may not classify accurately and may consume more time. There is a need to improve image classification accuracy on huge datasets while reducing processing time. Hence, we propose a novel ERCNN-DRM method, which makes the system work only on low dimensional data and outputs a regularized classification result.

The main contribution of the paper is as follows:

(i) When used on brain MRI images, pre-processing techniques in the existing systems, such as the median filter, Gaussian filter, and Gabor filter [20], resulted in blurred borders and edges and consumed a long time. Hence the bilateral filtering technique is used in the proposed system to overcome these drawbacks and enhance the performance rate.

(ii) The proposed technique improves the quality of the MRI images and sharpens the edges of the tumour area.
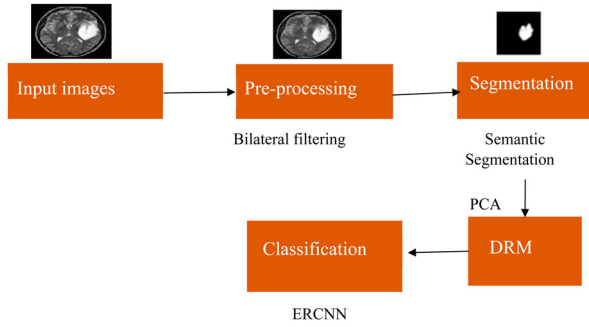
Figure 1. Workflow of the proposed methodology.

(iii) Several segmentation techniques in the existing systems [29] rely on certain parameters and statistical information and thus take longer. Without the use of any statistical information, the semantic segmentation technique easily detects the tumour since it is aware of the environment in which it works.

(iv) The dimension of the segmented region is reduced using an efficient *SEGMENTATION–PCA* algorithm and, therefore, only a lesser amount of data are required in the training model, thus reducing the complexity of the system.

(v) Also, to regularize the classification outputs, an efficient *REG–CNN* algorithm is proposed which regularizes the CNN classification and reduces the complexity of the architecture.

The paper is organized as follows: Introduction is depicted in Section 1. Section 2 shows the proposed methods, Section 3 shows the experimental results and Section 4 shows the conclusion.

2. Proposed methodology

Figure 1 explains the workflow of the proposed methodology. The entire process is carried out in four stages: Pre-processing, Segmentation, Feature Extraction, Dimensionality Reduction and Classification.

2.1. Dataset

The Cancer Imaging Archive (TCIA) Public Access repository was used to access brain MRI images, for the assessment of the proposed work [31]. This collection includes data from 20 patients that have recently been diagnosed with glioblastoma. It contains 696 MRIs, 224 of which are benign and 472 of which are malign. Each image is scaled at 224 × 224 pixels in a JPG/JPEG format.

2.2. Pre-processing

The bias fields cause MRI images to be damaged, due to the various intensity levels. The main aim of pre-processing is not only to remove the noise and

background data but also to enhance the image pixels. The techniques used in this process are classified into two types: frequency domain and spatial domain.

2.2.1. Bilateral filtering

Bilateral filtering is a spatial filter that smoothens the image and preserves the edges. It prevents averaging across the image edges and causes no loss in any image data. The proposed method prefers bilateral filtering, because of its non-iterative nature and its ability to maintain the sharpness of edges. The constraints needed in the noise removal process are window size w, standard deviation σ_d and σ_r has to be adjusted to the level of the noise. It uses a spatially weighted average in the edge smoothening process. In traditional low pass filtering, the pixel of a point is assumed to be equal to that of the pixel of nearby points:

$$_o(x) = k_d^{-1}(x)|| \int_{-\infty}^{\infty} i(\delta)c(\delta, x)_{d\delta} \tag{1}$$

where $(c(\delta, x))$ defines the geometric proximity between a neighbouring point x and the neighbourhood centre δ. Let i be input and o be output images and they might be multiband. In addition,

$$k_d(x) = || \int_{-\infty}^{\infty} c(\delta, x)_{d\delta} \tag{2}$$

The range of filtering is given as

$$_i(x) = k_r^{-1}(x)|| \int_{-\infty}^{\infty} o(\delta)s(o(\delta), o(x)_{d\delta} \tag{3}$$

where $((\delta), (x)$ computes the image resemblance among the pixel at the neighbourhood centre x and that of close by point δ. Here the kernel computes the similarity among pixels. The normalization constant is

$$_{k^r}^{-1}(x) = || \int_{-\infty}^{\infty} s(o(\delta), o(x)_{d\delta} \tag{4}$$

The bilateral filtering is described as given below:

$$_i(x) = k^{-1}(x)|| \int_{-\infty}^{\infty} o(\delta)c(\delta, x)s(o(\delta), o(x)_{d\delta} \tag{5}$$

where

$$k(x) = \int_{-\infty}^{\infty} c(\delta, x)o(o(\delta), o(x)_{d\delta} \tag{6}$$

Combined domain and range filtration is termed bilateral filtering.

2.3. Segmentation

To obtain ROI (Region of Interest) definition and recognition, many methods depend on segmentation performance. The original image is segmented into its constituent regions or subjects in medical image segmentation. It's also referred to as the image partition

process. In medical imaging equipment, segmentation is critical for extracting features from images, which are then used to analyze patients and these characteristics are useful for categorizing images into normal tissue and abnormal tissue.

2.3.1. Semantic segmentation

Our proposed system uses semantic segmentation since the technique is aware of the context of the area, in which it is working, say a tumour. The main aim of semantic segmentation [32] is to comprehend an image, down to the pixel level, marking each pixel with a class.

Several techniques discussed in the literature review find edges or gradients, but they never had a pixel-level perception of images in the way that humans do. Semantic segmentation solves this problem by grouping the parts of images that belong to the same object of interest. The algorithm is based on Faster-RCNN and the steps are as follows.

Algorithm 1: Semantic Segmentation

1. We take an image as input and pass it to the ConvNet, which returns the feature map for that image.
2. These feature maps are subjected to the Region Proposal Network (RPN). The object proposals are returned along with their objectness score.
3. These proposals are subjected to an ROI pooling layer, which reduces the size of all proposals to the same level.
4. Finally, the proposals are sent to a fully connected layer, which classifies and outputs bounding boxes for objects, where (i) the height of the box is the difference between the y coordinates of any top and bottom point, (ii) the width is the difference between the x-coordinates of any left or right point, (iii) the area of the box is the width times height, and (iv) the perimeter of the box is twice the width plus height.

The mean Dice coefficient was used as the measurement metric to evaluate the accuracy of segmentation. The formula is as follows:

$$\frac{2*|A \cap B|}{|A| + |B|} \tag{7}$$

where A is the predicted class of pixels and B is the ground truth.

2.4. The dimensionality reduction module

In image classification, the training phase consumes more time, as the dimension of the input data is high. The number of input variables in training data can be reduced, and the technique is referred to as dimensionality reduction. While using high-dimensional data, it is often beneficial to minimize dimensionality, by projecting the data to a lower-dimensional subspace that captures the data's identity. One of the most commonly used approaches to data analysis is dimensionality reduction using Principal Component Analysis (PCA) and its variants [33]. Once the image is subjected to PCA, only the relevant features from the segmented regions are extracted by deep learning techniques.

In this research, we propose an efficient algorithm called *SEGMENTATION–PCA* to reduce the dimension more efficiently than the optimum. The goal is to find a subspace L of dimension $m < d$, that minimizes the residual error of the points of Z projected onto L given a matrix Z_{n*d} with points as rows. The PCA algorithm generates a matrix Y of rank m and decomposes it into the orthogonal basis V of size m using the decomposition $Y = AV$ of Y. The eigenfaces are the images, produced by reducing the dimensionality of the segments. Using the PCA eigenfaces approach, each pixel is treated as an image with its dimension. The following is how the algorithm works:

Algorithm 2: *SEGMENTATION–PCA* (Dimensionality reduction)

Step 1: In the complete d-dimensional space, the optimal segmentation for sequence X is discovered. As a consequence, we have segments $S = (S_1, \dots , S_k)$ and d-dimensional vectors $u_1, \dots , u_k$ for each segment's points. The algorithm then considers the set of k vectors $u_1, \dots , u_k$, each of which is weighted by $|S_j|$, the length of segment S_j.

Step 2: Let $U_s = (u_1, |S_1|), \dots , (u_k, |S_k|)$ denote this set of weighted vectors. Intuitively, the set U_s is a set of n d-dimensional points that approximate the k d-dimensional points of the sequence X.

Step 3: We perform PCA on the collection of weighted points U_s to reduce the dimensionality from d to m. For each segment vector u_j, the PCA computation yields an approximate representation u_j' such that $u_j' = \sum n_t = 1.a_{jt}.v_t, j = 1, \dots , k$ (4.1) where $v_1, \dots , v_m$ constitute a basis, and a_{jt} are real-valued coefficients.

Step 4: The vectors $u_1', \dots , u_k'$ in Equation (4.1) are in an m-dimensional space, and the weighted PCA's optimality ensures that they minimize the error P of all possible k vectors in m-dimensional space.

Step 5: The final step of the *SEGMENTATION–PCA* algorithm is to assign the vector u_j' computed by PCA to each segment S_j.

Step 6: The output is dimensional reduced segments for feature extraction.

In contrast to traditional PCA, the proposed algorithm employs the mean of each class rather than the specific image within the class. Because each class's average is a linear combination of within-class images, it retains several variations of the specific image. In other words, each image's compression process is more advantageous to image recognition. Furthermore, another important benefit of the improved PCA is that training time is highly reduced.

2.5. Proposed classification technique (ERCNN)

After the dimensional reduced features from the brain region have been extracted, a few algorithms are used to classify the images into their respective regions, and they are referred to as classifiers. CNN is a common deep learning classification architecture. Convolutional Neural networks (CNNs)-based applications have become wide, where proper regularization is greatly needed. The CNNs are composed of a large number of layers, units, and connections relevant to their complex structure, and various filters in each convolutional layer. This is susceptible to overfitting, which is a major issue. Overfitting occurs when a model attempts to predict a general pattern in noisy data. This is the result of an overly complex model, with
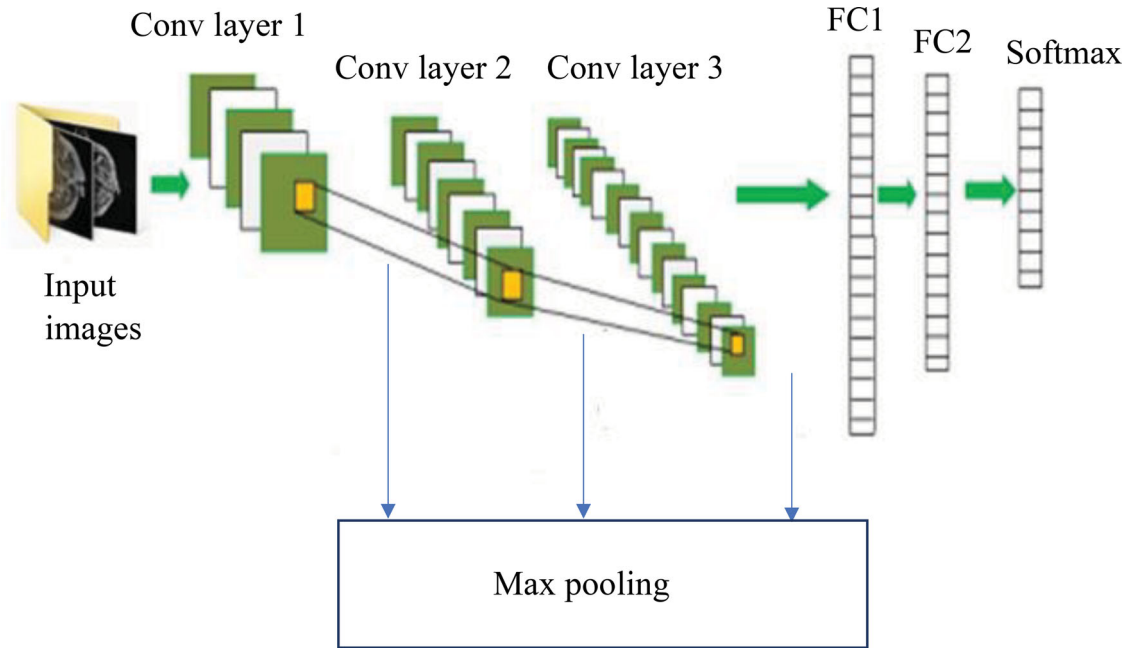
Figure 2. CNN architecture.

an excessive number of parameters. Overfitted models are inaccurate because the pattern does not reflect the reality present in the data. Several regularization approaches, such as data augmentation, Dropout and batch normalization, group normalization, Layer normalization, and Instance Normalization [34], have been designed to address this issue and increase CNN efficiency while reducing overfitting. In this paper, we propose an efficient Regularized CNN, which drops out random nodes during training. A single model works on several different network architectures. The idea behind this regularization approach is that, with each training, the network learns with fewer nodes, thereby reducing complexity. Thus, it reduces overfitting and improves generalization error in deep neural networks. It is cheap and efficient in terms of computation. We propose a novel algorithm *REG–CNN* to perform regularization. The proposed strategy differs from the conventional dropout [35] in that it attempts to block out the most active neurons, which are responsible for producing sparsity in the model, at the point where the hidden neurons are encouraged to acquire more relevant features and extract usable information. This improves the network's ability to generalize. The steps are as follows:

Algorithm 3: *REG_CNN Algorithm*

1: while training do
2: for each hidden layer do
3: rate ← *U*(0, *r*)
4: normTensor ← L2Normalize(Tensor)
5: max ← Max(normTensor)
6: keptIdx ← IdxOf(normTensor, (1 − rate) * max)
7: returnTensor ← Tensor * KeptIdx
8: end for
9: end while

Each layer's output yields a $x \times y \times z$ tensor, where the image size is represented by x and y, and the number of feature maps produced for each convolutional kernel is denoted by z. Step 6 builds a new tensor with the same shape as the input one and assigns 1 where $(1 − \text{rate}) \times \text{max}$ is larger than a certain threshold at a specific tensor point; otherwise, it sets that place to 0.
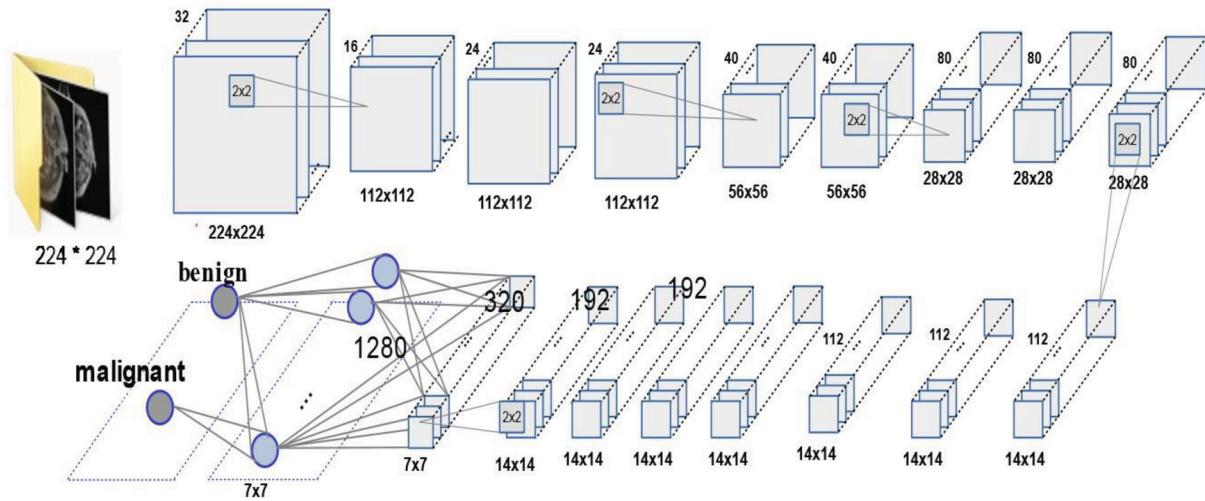
2.5.1. CNN architecture

The CNN architecture is made up of six layers: three convolutional layers accompanied by a max pooling layer, two completely connected layers and the softmax layer. The architecture of the CNN is shown in Figure 2.

2.5.2. Layer description

Convolutional layer. The first layer is used for feature extraction from input images. The convolution operation is performed in the input image, and then the resultant is passed to the following layer. The feature map is obtained by the dot product between the filter, and the sections of the input image with respect to the filter size are taken, by sliding the filter over the input image, and it contains details about the corners and edges of an image. Then the feature map is fed to other layers, to learn other features from the input image. Each convolutional layer is accompanied by a max pooling layer. The calculation of the features of the convolutional layers is obtained using

$$ynl = fl(\sum m \to nlyml − 1),$$

where y_n^l the nth feature map of l-layer, $m \to l_n$ is C-kernel, while feature extraction from layer-l, and $y_{m^{l-1}}$ is the characteristic patterns linked to layer-l.

Figure 3. ResNet-50 architecture.

Max pooling layer. Maximum pooling, also known as max pooling, is a pooling process that decides the maximum value in each function map region. The result is a collection of down-sampled feature maps which show the region's most prominent feature.

Fully connected layer. The Fully Connected (FC) layer is the layer found, before the output layer. It connects the neurons between two different layers. Here, the flattened output from the previous layer is fed as the input. The classification process begins to take place at this phase. The proposed method uses two completely connected layers with 600 and 300 units performed after the convolutional layers.

Dropout layer. It is used to regularize the classification. On the first, second, and third convolutional layers, and two completely connected layers, a dropout layer with a probability of 0.5 is added to the output.

Softmax layer. The Softmax layer is the last layer in CNN. It is used to classify the images into different classes. The output of the layer is classified as benign and malign tumours.

2.5.3. Training model
ResNet-50. Figure 3 describes the ResNet-50 architecture. It's Kaiming He et al.'s 50-layer Residual Network from Microsoft Research [36]. Feature transformation is referred to as residual. It corresponds to the features that that layer learns from its input.

ResNet accomplishes this using shortcut connections (connecting the input of the mth layer directly to the input of some $(m+x)^h$ layer). Compared to conventional networks, these networks are much easier to train. It also improves accuracy. The input image each of size 224×224 is analyzed. To reduce the feature map size, the next layers are of lower scale in resolution

Table 1. Data split-up.

Type of tumour	Total images	Training images	Testing images	Validation images
Benign	224	74	75	75
Malign	472	252	75	145

and to increase accuracy it is the upper scale in width. ResNet-50 has fewer parameters and high accuracy.

3. Simulation results and discussion

This section deals with the obtained results, and its discussion of brain tumour classification. ERCNN DRM is performed on the brain MRI to detect and classify the tumorous images into benign and malign. We experimented on brain tumour MRI from the TCIA dataset [31]. This collection includes data from 20 patients, who have recently been diagnosed with tumours. It holds 696 MRIs, 224 of which are benign and 472 of which are malign. We split our data into training, validation, and testing, as shown in Table 1, to evaluate our model accuracy. The experiment is done using MATLAB 2020 on a CPU 2.3 GHz core i5 processor with 8 Gb of ram. Our proposed model showed 97% accuracy in our training data and 96.7% accuracy in our validation dataset. The following steps show the results obtained from the brain MRI from the database.
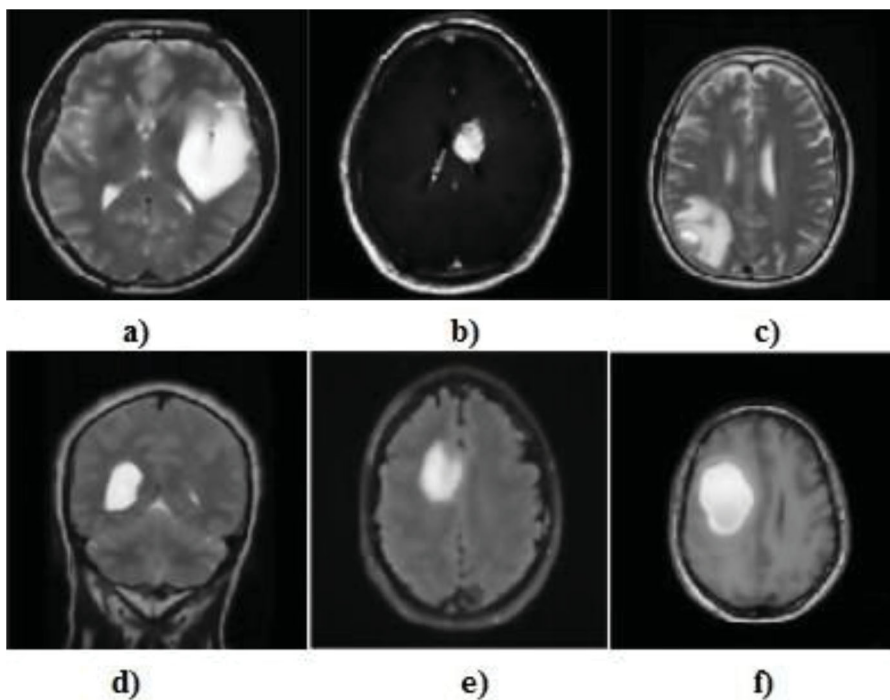
3.1. Pre-processing

The MRI images are subjected to the pre-processing method, to improve the contrast and the quality of the image. Figure 4 shows the input images.

In the proposed system, bilateral filtering is used for pre-processing brain MRI images. The filter smoothens and sharpens the edges of the images, as shown in Figure 5. Once the pre-processing techniques is applied, the pixel quality of the image is increased and further subjected to segmentation.
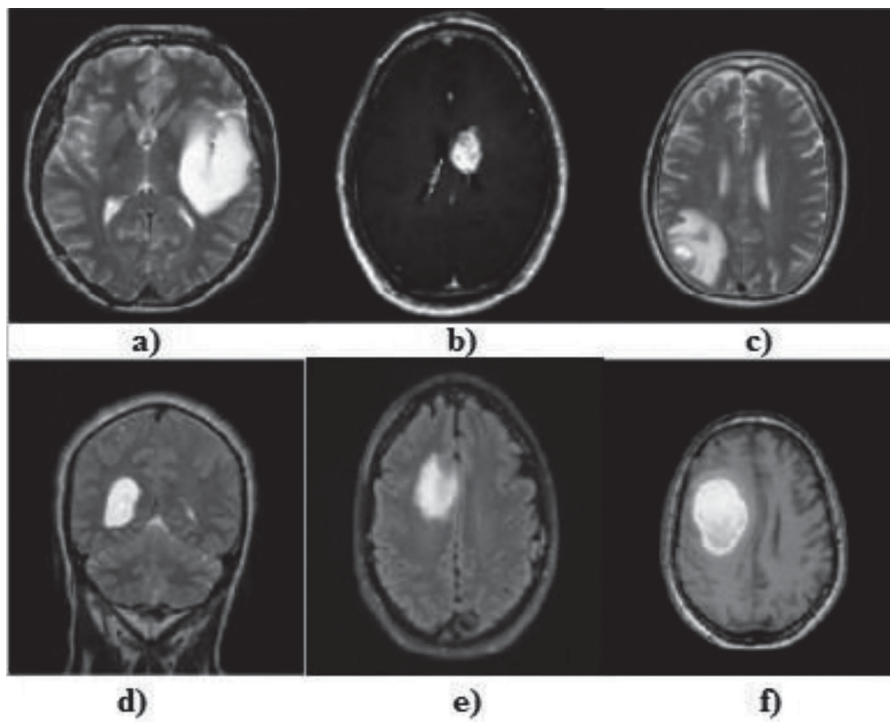
Figure 4. Input image.

Figure 5. Pre-processed image.

3.2. Segmentation

Following the pre-processing, the obtained image is fed to the segmentation method, to segment the tumorous area from the brain tumour MRI. Semantic segmentation performs segmentation by recognizing the object at first using a bounding box, as shown in Figure 6, and then segments the tumour portion, as shown in Figure 7.

3.3. Classification

Following the segmentation, the segmented features are dimensionally reduced using PCA operations and then fed into the CNN classifier, which then classifies the brain images into benign and malign. The parameters used in the CNN architecture are given in Table 2.

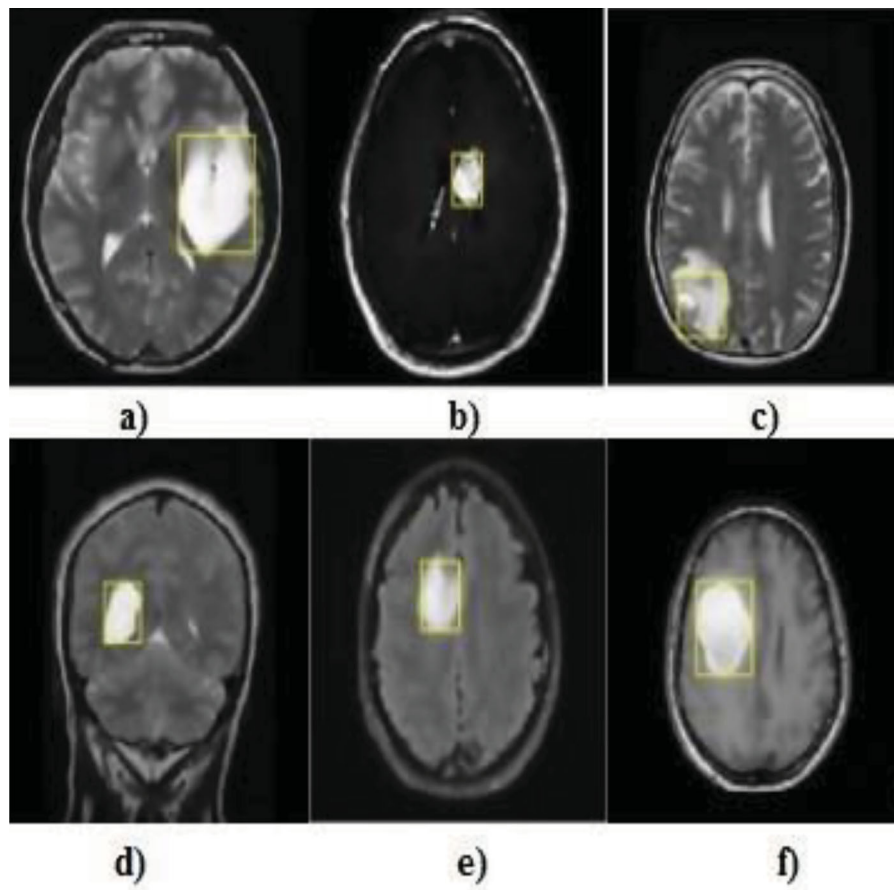The confusion matrix obtained during the simulation process is shown in Table 3.
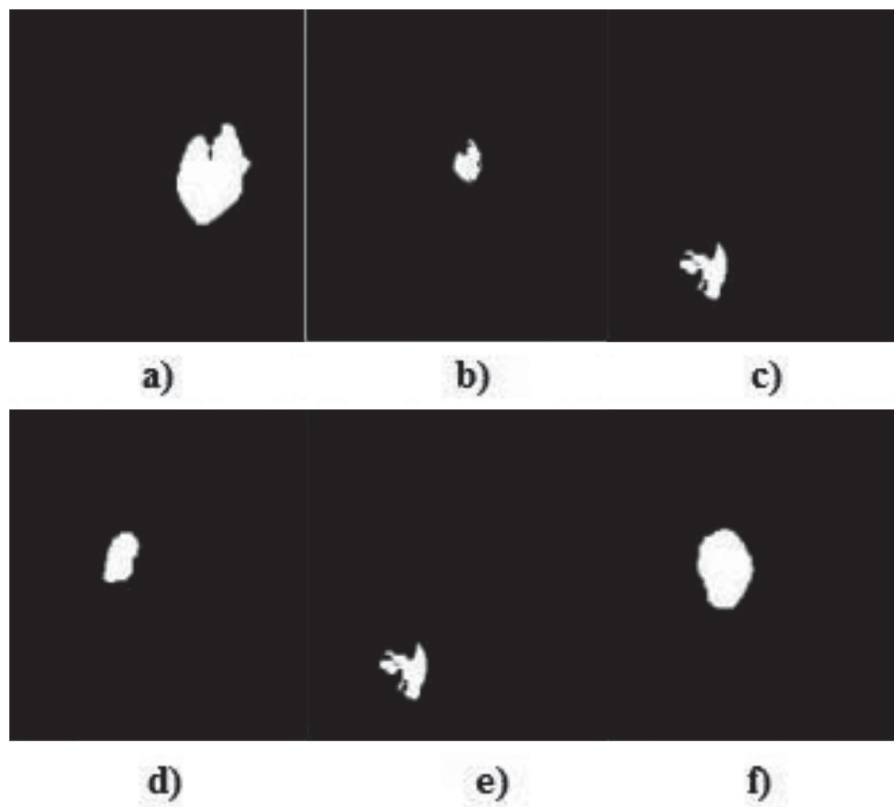
Figure 6. Object recognition.

Figure 7. Segmented tumour.

Table 2. Parameters of CNN layers.

Layer	Filter size
Convolutional layers	15, 20, 25 with size 5×5
Max pooling layer	2×2
Fully connected layers	600 and 300 units

Table 3. Confusion matrix.

Output class	Benign	73 TP (48.7%)	3 FP (2%)	96.1% PPV
	Malign	2 FN (1.3%)	72 TN (48%)	97.3% NPV
		97.3% Sensitivity	96.0% Specificity	96.7% Accuracy
		Benign	Malign	
			Target class	

In Table 3 among 75 benign cases, 73 cases are correctly classified as benign (TP), while two of them are misclassified as malignant (FN). Among 75 malignant cases, used for testing 72 cases are correctly classified as malign (TN), while three of them are misclassified as benign (FP). The percentage of TPs obtained using the proposed work is 48.7%, the percentage of FPs obtained is 2%, the percentage of FNs obtained is 1.3%, and the percentage of TNs obtained is 48%. The accuracy of classifying the tumours into benign and malign, using the proposed work is 96.7%.

3.4. Performance metrices

True positive (TP): In the case of a tumour input, the test would be positive.

True negative (TN): In the case of a non-tumour input, the test would be negative.

False positive (FP): In the case of a non-tumour input, the result is positive.

False negative (FN): In the case of a tumour input, the result would be negative.

Accuracy: The amount of perfect recognition of tumour in the MRI a, b, c, d, e and f.

$$\text{Accuracy} = a + b/c + d$$

Sensitivity (TPR): The sum of positive results predicted accurately is called a True Positive Rate (TPR).

$$\text{TPR} = a/a + d$$

Specificity (TNR): The total of negatives predicted accurately is the True Negative Rate (TNR).

$$\text{TNR} = b/b + c$$

Precision: The percentage of expected positives that are true positives.

$$PPV = a/a + c$$

F-measure: The average of precision and sensitivity.

$$F - \text{measure} = 2a/a + c + d$$

Table 4. Segmentation evaluation.

Methods	Dice coefficient
K-Means [40]	0.6710
Rough Fuzzy C-Means [41]	0.7722
OUAT [42]	0.6239
Proposed	0.8970

False-positive rate (FPR): The fraction of all negatives still provides positive test outcomes.

$$\text{FPR} = c/c + b$$

False-negative rate (FNR): The percentage of positives still provides negative test outcomes.

$$\text{FNR} = d/d + a$$

Balanced error rate (BER): The moderate error rate on the positive and negative outcomes.

$$\text{BER} = 1 - 0.5 \times ((\text{sensitivity} + \text{specificity}) / 100)$$

Negative predictive value (NPV): The outcome is positive instead of a negative result.

$$\text{NPV} = b/b + d,$$

where a and b are the true positive and true negative results and c and d are the false positive and false negative values, respectively.

3.5. Performance analysis

The performance analysis for the pre-processing method, proposed segmentation algorithm, proposed dimensionality reduction algorithm, proposed regularization and the CNN classification is done by comparing with other existing methods in this section. Furthermore, statistical analysis using the Friedman test and Post-Hoc Holm procedure is done to show the superiority of the proposed system over other systems.

3.5.1. Segmentation analysis
Dice coefficient. The Dice coefficient is used to analyze the correctness of the segmentation results.

Table 4 tabulates the segmentation accuracy for various algorithms, namely, K-Means, Rough Fuzzy C-Means (RFCM), optimized U-Net and adaptive thresholding (OUAT) algorithms and the semantic segmentation used in the proposed system, which are evaluated using the Dice Coefficient.

Table 4 shows the segmentation accuracy obtained from various methods, such as K-Means, RFCM and OUAT algorithms. The Dice Coefficient value (0.89) obtained from the proposed work is more significant than other methods.

Furthermore, the segmentation time for testing data is described in Table 5. The computational performance of four existing methods and the proposed method is studied.

Table 5. Comparative analysis of segmentation time of different methods.

Works	Processing time
Pereira et al. [43]	8 s–24 min
Havaei et al. [44]	8 min
Kamnitsas et al. [45]	30 s
Dong et al. [46]	2–3 s
Proposed	1.80 s
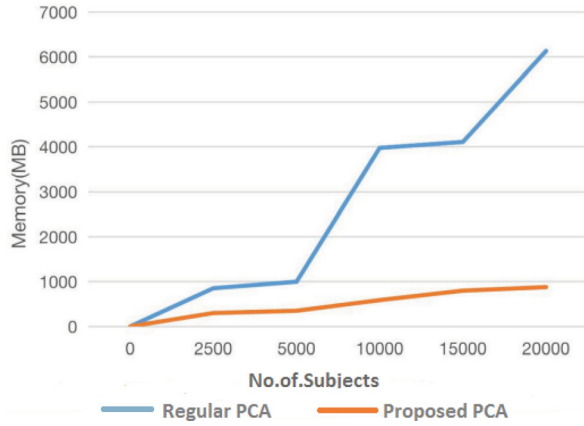
Figure 8. Comparison of the regular PCA and proposed PCA.

Table 6. Training parameters.

No. of Epochs	50
Batch size	20
Dropout rate	0.5
Learning rate	0.001

Table 7. Performance comparison of conventional and proposed dropout regularization methods.

Parameters	Conventional dropout	Proposed dropout
Training accuracy	0.867	0.916
Training loss	0.359	0.294
Test accuracy	0.821	0.918

The segmentation techniques proposed by various authors and the proposed technique are studied and tabulated in Table 5. The semantic segmentation used in the proposed system takes 1.80 s, which is comparatively more significant than other systems illustrated in Table 5.

Performance analysis of regular PCA and our proposed SEGMENTATION-PCA. The proposed SEGMENTATION_PCA algorithm is compared with the existing PCA and the result is shown in Figure 8.

Figure 8 shows that the proposed PCA technique requires less memory than the existing PCA technique.

3.5.2. Classification analysis

Table 6 shows the training parameters considered to simulate the proposed system.

Performance analysis of the proposed dropout regularization methods. Table 7 shows the performance comparison of conventional and proposed dropout regularization methods.

Table 8. Comparison of BER and NPV.

Parameters	BER	NPV
Proposed	0.013	0.973
ANN [47]	0.09	0.79
Multi-SVM [48]	0.13	0.6
KNN [49]	0.18	0.57

Table 7 shows the loss for the proposed method, and our proposed method achieved a lower loss of 0.294, training accuracy of 0.916 and test accuracy of 0.918.

Sensitivity and specificity. The sensitivity and specificity of various methods are compared with the proposed method and shown in Figure 9.

Figure 9 represents the performance comparison of the proposed scheme with different methods, such as ANN, Multi SVM, and KNN. The performance of specificity and sensitivity are analyzed for the proposed approach and other methods. Figure 9 shows that the proposed method achieved better sensitivity (97.3%) and specificity (96%) rates than other methods.

Precision and F-measure. Figure 10 shows the precision and F-Measure comparison of the proposed scheme with different methods, such as ANN, Multi SVM, KNN. Figure 10 shows that the proposed approach achieved better precision (94.8%) and F-Measure (95.8%) rates than those of other methods.

FPR and FNR. Figure 11 represents the FPR and FNR comparison of the proposed scheme with different methods, such as ANN, Multi SVM, and KNN. Figure 10 shows that the proposed approach achieved the better FPR (0.424) and FNR (0.029) rates than those of other methods.
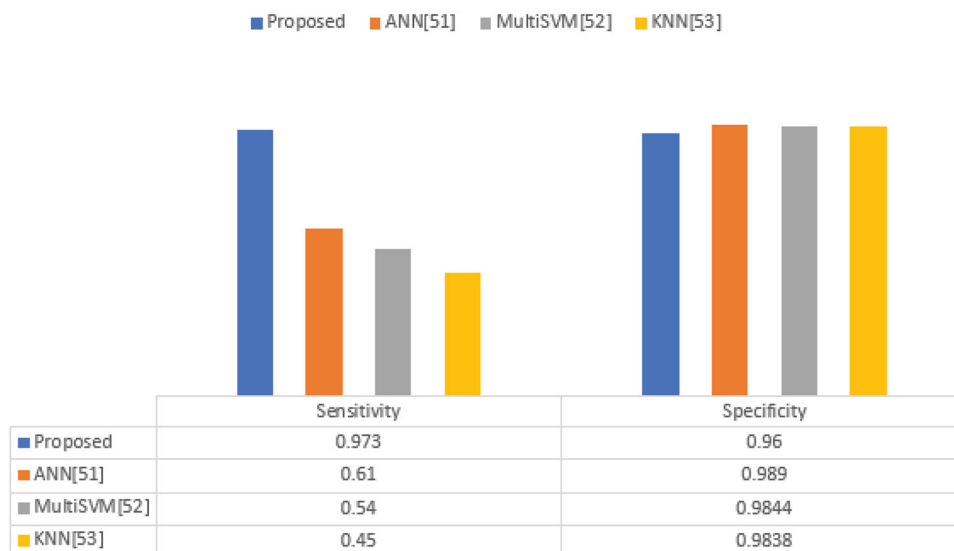
BER and NPV. Table 8 represents the BER and NPV comparison of the proposed scheme with different methods, such as ANN, Multi SVM, and KNN. It shows that the proposed approach achieved better BER (0.013) and NPV (0.973) rates than those of other methods.

Accuracy vs. Epoch. Figure 12 describes the accuracy vs. epoch graph obtained during the training and validation phase. It proves that the proposed system is highly significant.

Loss vs. Epoch. Figure 13 describes the loss vs. epoch graph obtained, during the training and validation phase. It proves that the proposed system is highly significant.
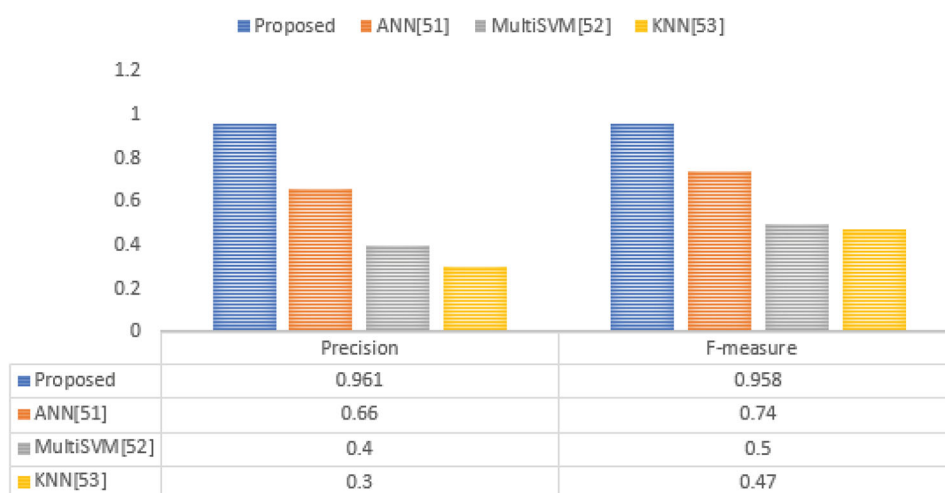
Comparative analysis of the accuracy of different state-of-the-art methods. The comparative analysis of the accuracy of different state-of-the-art methods and the proposed method using various protocols is shown in Table 9.

SENSITIVITY AND SPECIFICITY

■ Proposed ■ ANN[51] ■ MultiSVM[52] ■ KNN[53]

	Sensitivity	Specificity
■ Proposed	0.973	0.96
■ ANN[51]	0.61	0.989
■ MultiSVM[52]	0.54	0.9844
■ KNN[53]	0.45	0.9838

Figure 9. Sensitivity and specificity graph for a different scheme.

PRECISION AND F-MEASURE

■ Proposed ■ ANN[51] ■ MultiSVM[52] ■ KNN[53]

|	Precision	F-measure
■ Proposed	0.961	0.958
■ ANN[51]	0.66	0.74
■ MultiSVM[52]	0.4	0.5
■ KNN[53]	0.3	0.47

Figure 10. Precision and F-measure comparison.

Table 9 shows that the proposed scheme provides an accuracy rate of 96.7% which is more significant than other state-of-the-art methods. The proposed ERCNN-DRM used to classify the brain images provides better results than other state-of-the-art methods.

*ROC curves.* Figure 14 shows the area under the ROC curve (AUC) Ac, which is a valuable metric for determining how well a device can differentiate between two diagnostic classes. Figure 14 shows the ROC curves obtained using different deep learning methods. The region (Ac) under the ROC curve of the proposed ERCNN method is greater than that of other approaches, implying that it is closer to 1 than others. As a result, the suggested approach has the greatest ability to distinguish.

**Table 9.** Comparative analysis of the accuracy of different state-of-the-art methods.

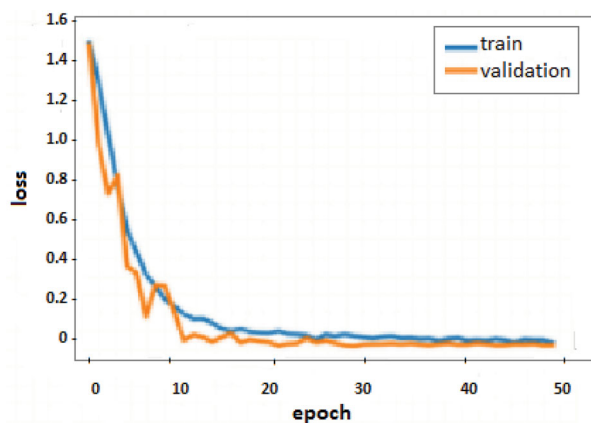| Name of authors	MRI protocols	Validation protocols	Dataset	Accuracy (%)
Hasan and Linte [50]	Brain	U-Net DCNN	BRATS	91
Prabhu and Jayachandran [51]	Brain	Hybrid SVM	Unknown	91.6
Ratna et al. [39]	Brain	Multi-SVNN	BRATS	93
Malathi and Sinthia [52]	Brain	BPN	Unknown	93
Proposed	Brain	ERCNN	TCIA	96.7
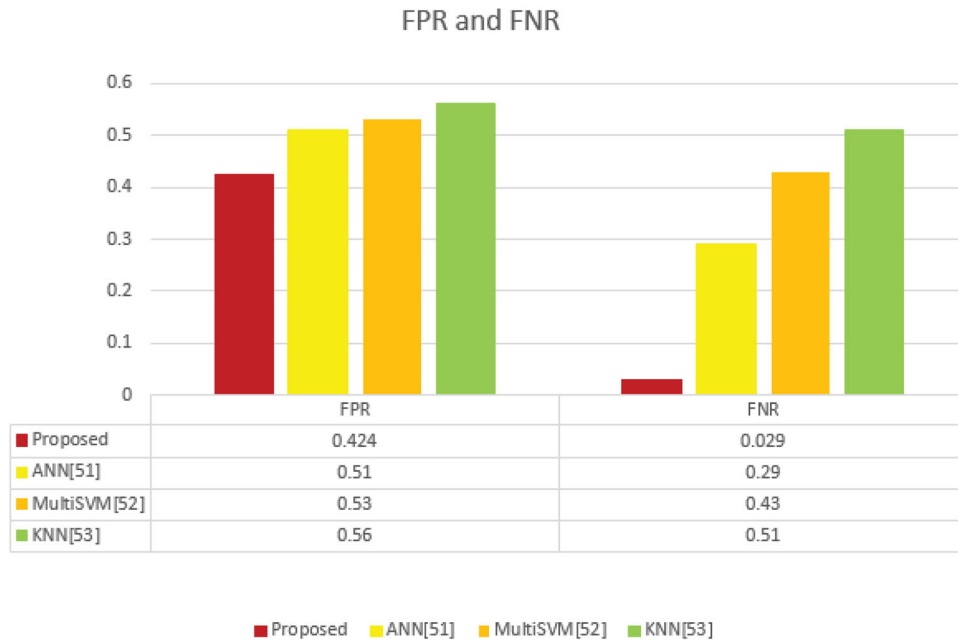
Figure 11. FPR and FNR comparison.
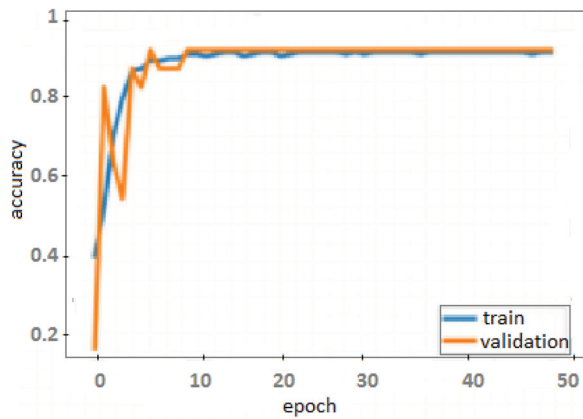
Figure 12. Accuracy vs. Epoch graph.
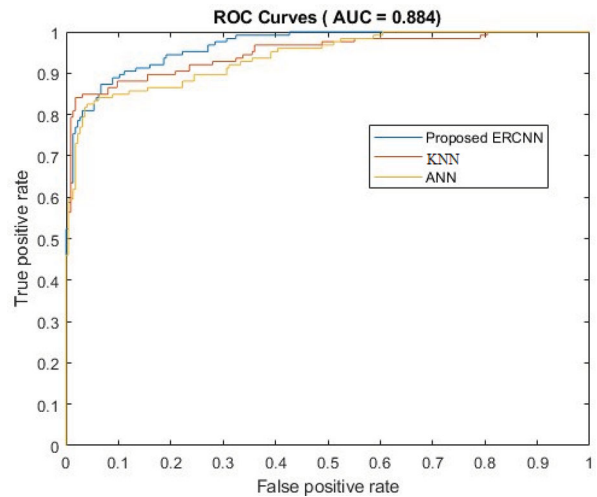
Figure 13. Loss vs. Epoch graph.

Figure 14. ROC AUC curve.

Table 10. FAR rank based on the AUC curve.

Methods	FAR rank
Proposed	3.11
KNN [49]	7.5
ANN [47]	9.7

3.6. Statistical analysis

3.6.1. Friedman aligned ranking (FAR)

To statistically verify the superiority of the proposed method, we utilized the non-parametric Friedman aligned ranking (FAR) test [37]. FAR test based on the area under curve (AUC) metric is analyzed and listed in Table 10. The null hypothesis (H0) is stated as H0: There is no such significant variation among all the models, i.e. all the models are equivalent, alternatively, the alternative hypothesis (H1) contradicts the same. Here, the Friedman test has been conducted for the statistical significance of the models. In Friedman Test, each model is assigned a rank based on the AUC of the models. The highest rank is assigned with the smallest number and the lowest rank is assigned with the highest number.

Table 11. Post-Hoc Holm test.

Methods	Unadjusted p-value
Proposed	.147299
KNN [49]	.09769
ANN [47]	.000084

Table 10 shows that the proposed system performed well than the other existing methods such as KNN and ANN. The proposed system has obtained a better ranking (3.11).

The Post-Hoc test experiment has been conducted after the rejection of the null hypothesis using the Holm procedure. The Holm procedure [38] computes the performance of each model with others using z-value and p-value. However, after applying the Holm test, we obtained the results, as shown in Table 11.

From Table 11, we can observe that the Holm test rejected the hypothesis with unadjusted p-values smaller than 0.001213. Therefore, neither the proposed method nor the KNN was rejected. On the contrary, only the ANN network was rejected, showing significant differences (inferior performance) compared with the other algorithms.

4. Conclusion

This paper proposes an improved accurate and automated system for recognizing benign and malign brain cancers through MRI classification. The proposed system uses bilateral filtering for pre-processing of brain tumour MRI. The outputs from the segmentation technique show that the semantic segmentation technique provides better results than other existing methods discussed in the literature. Then the segmented region was supposed to a dimensionality reduction technique to reduce the complexity of the classification process. Finally, the proposed ERCNN is used to classify the images into benign or malign. The proposed system ERCNN-DRM reduces the complexity of the system by working on reduced dimensional data. The performance of the proposed classifier and various methods, such as ANN, Multi SVM and KNN is compared, and it is found that the accuracy obtained through the proposed system is 96.7% which is higher than that of the existing classification techniques, as discussed in the literature. It is found that the proposed method was more accurate to classify images through the CAD system.

Disclosure statement

No potential conflict of interest was reported by the author(s).

References

[1] Kaldera HNTK, Gunasekara SR, Dissanayake MB. Brain tumor classification and segmentation using faster RCNN. 2019 Advances in Science and Engineering Technology International Conferences (ASET): IEEE; 2019; p. 1–6.

[2] Harish P, Baskar S. MRI based detection and classification of brain tumor using enhanced faster R-CNN and Alex Net model. Materials Today: Proceedings; 2020.

[3] Anaraki AK, Ayati M, Kazemi F. Magnetic resonance imaging-based brain tumor grades classification and grading via convolutional neural networks and genetic algorithms. Biocybern Biomed Eng. 2019;39(1):63–74.

[4] Rao CR, Kumar MNVSS, Rao GSB. A novel segmentation algorithm for feature extraction of brain MRI tumour. Inf Decis Sci. 2018: 455–463.

[5] Latha M, Surya R. Brain tumour detection using neural network classifier and kmeans clustering algorithm for classification and segmentation. Brain. 2016;1(01): 27–32.

[6] Rajesh T, Suja Mani Malar R, Geetha MR. Brain tumor detection using optimisation classification based on rough set theory. Cluster Comput. 2019;22(6): 13853–13859.

[7] Desai D, Chapatwala N. Brain extraction methods for magnetic resonance images (MRI). Brain. 2016;4(5).

[8] Sajjad M, Khan S, Jan Z, et al. Leukocytes classification and segmentation in microscopic blood smear: a resource-aware healthcare service in smart cities. IEEE Access. 2017;5:3475–3489.

[9] Jan Z, Khan A, Sajjad M, et al. A review on automated diagnosis of malaria parasite in microscopic blood smears images. Multimed Tools Appl. 2018;77: 9801–9826.

[10] Elhoseny M, Abdelaziz A, Salama AS, et al. A hybrid model of internet of things and cloud computing to manage big data in health services applications. Future Gener Comput Syst. 2018;86:1383–1394.

[11] Menze H, Jakab A, Bauer S, et al. The multimodal brain tumor image segmentation benchmark (BRATS). IEEE Trans Med Imaging. 2015;34:1993.

[12] Siva Raja, PM, Rani AV. Brain tumor classification using a hybrid deep autoencoder with Bayesian fuzzy clustering-based segmentation approach. Biocybern Biomed Eng. 2020;40(1).

[13] Gao H, Xiao J, Yin Y, et al. A mutually supervised graph attention network for few-shot segmentation: the perspective of fully utilizing limited samples. IEEE Trans Neural Netw Learn Syst. 2022.

[14] Gao H, Xu K, Cao M, et al. The deep features and attention mechanism-based method to dish healthcare under social IoT systems: an empirical study with a hand-deep local-global net. IEEE Trans Comput Soc Syst. 2021;(1): 336–347.

[15] Xiao J, Xu H, Gao H, et al. A weakly supervised semantic segmentation network by aggregating seed cues: the multi-object proposal generation perspective. ACM Trans Multimid Comput Commun Appl. 2021;17(1s):1–19.

[16] Chen J, Ying H, Liu X, et al. A transfer learning based super-resolution microscopy for biopsy slice images: the joint methods perspective. IEEE/ACM Trans Comput Biol Bioinf. 2020;18(1):103–113.

[17] Chen T, Liu X, Feng R, et al. Discriminative cervical lesion detection in colposcopic images with global class activation and local bin excitation. IEEE J Biomed Health Inform. 2021.

[18] Feng R, Cao Y, Liu X, et al. Chronet: a multi-task learning based approach for prediction of multiple chronic diseases. Multimed Tools Appl. 2021: 1–15.

[19] Mishra SK. Brain image classification using dual tree MBand wavelet transforms and support vector machine. Indian J Public Health Res Dev. 2019;10(11).

[20] Shen G, Ding Y, Lan T, et al. Brain tumor segmentation using concurrent fully convolutional networks and conditional random fields. Proceedings of the 3rd International Conference on Multimedia and Image Processing; 2018. p. 24–30.

[21] Litjens G, Kooi T, Bejnordi BE, et al. "A survey on deep learning in medical image analysis". Med Image Anal. 2017;42:60–88.

[22] Badža MM, Marko ČB. Classification of brain tumors from MRI images using a convolutional neural network. Appl Sci. 2020;10(6):1999.

[23] Díaz-Pernas FJ, Martínez-Zarzuela M, AntónRodríguez M, et al. A deep learning approach for brain tumor classification and segmentation using a multiscale convolutional neural network. Healthcare. 2021;9(2):153.

[24] Razzak MI, Imran M, Xu G. Efficient brain tumor segmentation with multiscale two-pathway-group conventional neural networks. IEEE J Biomed Health Inform. 2018;23(5):1911–1919.

[25] Cui Z, Chen W, Chen Y. Multi-scale convolutional neural networks for time series classification. arXiv preprint arXiv:1603.06995. 2016.

[26] Alhichri H, Alajlan N, Bazi Y, et al. Multiscale convolutional neural network for remote sensing scene classification. 2018 IEEE International Conference on Electro/Information Technology (EIT): IEEE; 2018. p. 1–5.

[27] Chelghoum R, Ikhlef A, Hameurlaine A, et al. Transfer learning using convolutional neural network architectures for brain tumor classification from MRI images. IFIP international Conference on Artificial Intelligence Applications and Innovations; Cham: Springer; 2020. p. 189–200.

[28] Das S, Rahman Aranya OR, Labiba NN. Brain tumor classification using convolutional neural network. 2019 1st International Conference on Advances in Science, Engineering and Robotics Technology (ICASERT): IEEE; 2019. p. 1–5.

[29] Sriramakrishnan P, Kalaiselvi T, Rajeswaran R. Modified local ternary patterns technique for brain tumour segmentation and volume estimation from MRI multisequence scans with GPU CUDA machine. Biocybern Biomed Eng. 2019;39(2):470–487.

[30] Al-Tamimi MSH, Hmoud Al-Tamimi AS, Sulong G. A new abnormality detection approach for T1-weighted magnetic resonance imaging brain slices using three planes. Adv Comput. 2016;6(1):6–27.

[31] Clark K, Vendt B, Smith K, et al. The cancer imaging archive (TCIA): maintaining and operating a public information repository. J Digit Imaging. 2013;26(6):1045–1057.

[32] Martinez-Soltero G, Alanis AY, Arana-Daniel N, et al. Semantic segmentation for aerial mapping. Mathematics. 2020;8(9):1456.

[33] Garg I, Panda P, Roy K. A low effort approach to structured CNN design using PCA. IEEE Access. 2019;8:1347–1360.

[34] Budak C, Mençik V, Emin ASKER M. Effect on model performance of regularization methods. Dicle Üniversitesi Mühendislik Fakültesi Mühendislik Dergisi. 2021;12(5):757–765.

[35] Srivastava N, et al. Dropout: a simple way to prevent neural networks from overfitting. J Mach Learn Res. 2014;15(1):1929–1958.

[36] He K, Zhang X, Ren S, et al. Deep residual learning for image recognition. Proceedings of the IEEE Conference on Computer Vision and Pattern Recognition; 2016. p. 770–778.

[37] Derrac J, García S, Molina D, et al. A practical tutorial on the use of nonparametric statistical tests as a methodology for comparing evolutionary and swarm intelligence algorithms. Swarm Evol Comput. 2011;1(1):3–18.

[38] Holm S. A simple sequentially rejective multiple test procedure. Scand J Stat. 1979: 65–70.

[39] Raju AR, Suresh P, Rajeswara Rao R. Bayesian HCS-based multi-SVNN: a classification approach for brain tumor segmentation and classification using Bayesian fuzzy clustering. Biocybern Biomed Eng. 2018;38(3):646–660.

[40] Aslam HA, Ali Ahsan MI, Ramashri T. A new approach to image segmentation for brain tumour detection using pillar K-means algorithm. Int J Adv Res Comput Commun Eng. 2013;2:1429–1436.

[41] Maji P, Pal SK. RFCM: a hybrid clustering algorithm using rough and fuzzy sets. Fundam Inform. 2007;80:475496.

[42] Venkateswarlu Isunuri B, Kakarla J. Fast brain tumour segmentation using optimized U-Net and adaptive thresholding; 2020.

[43] Pereira S, Pinto A, Alves V, et al. Brain tumor segmentation using convolutional neural networks in MRI images. IEEE Trans Med Imaging. 2016;35(5):1240–1251.

[44] Havaei M, Davy A, Warde-Farley D, et al. Brain tumor segmentation with deep neural networks. Med Image Anal. 2017;35:18–31.

[45] Kamnitsas K, Ledig C, Newcombe VFJ, et al. Efficient multi-scale 3D CNN with fully connected CRF for accurate brain lesion segmentation. Med Image Anal. 2017;36:61–78.

[46] Dong H, Yang G, Liu F, et al. Automatic brain tumor detection and segmentation using U-net based fully convolutional networks, medical image understanding and analysis. MIUA 2017. Commun Comput Inf Sci. 2017;723:506–517.

[47] Chavan NV, Jadhav BD, Patil PM. Detection and classification of brain tumors. Int J Comput Appl. 2015;112(8).

[48] Suhag S, Saini LM. Automatic brain tumor detection and classification using an SVM classifier. Proceedings of ISER 2nd International Conference; 2015. p. 55–59.

[49] Deepa SN, Devi BA. Artificial neural networks design for the classification of brain tumors. Computer Communication and Informatics (ICCCI), 2012 International Conference on IEEE; 2012. p. 1–6.

[50] Hasan SK, Linte CA. A modified U-Net convolutional network featuring a nearest-neighbor Re-sampling-based elastic transformation for brain tissue characterization and segmentation. 2018 IEEE Western New York Image and Signal Processing Workshop (WNYISPW): IEEE; 2018. p. 1–5.

[51] Prabhu LAJ, Jayachandran A. Mixture model segmentation system for parasagittal meningioma brain tumor classification based on hybrid feature vector. J Med Syst. 2018;42(12):1–6.

[52] Malathi M, Sinthia P. MRI brain tumour segmentation using hybrid clustering and classification by back propagation algorithm. Asian Pac J Cancer Prev: APJCP. 2018;19(11):3257–3263.